PERGAMON

Journal of Atmospheric and Solar-Terrestrial Physics 62 (2000) 947–954

Journal of ATMOSPHERIC AND SOLAR-TERRESTRIAL PHYSICS

# Global energy deposition to the topside ionosphere from superthermal electrons

G.V. Khazanov[a], M.W. Liemohn[b,*], J.U. Kozyra[b], D.L. Gallagher[c]

[a]*Geophysical Institute and Physics Department, University of Alaska Fairbanks, Fairbanks, AK 99775, USA*
[b]*Department of Atmospheric, Oceanic and Space Sciences, Space Physics Research Laboratory, University of Michigan, 2455 Hayward Street, Ann Arbor, MI 48109, USA*
[c]*Space Sciences Laboratory, NASA Marshall Space Flight Center, Huntsville, AL 35812, USA*

Received 12 August 1999; accepted 20 October 1999

**Abstract**

The subauroral heat input to the topside ionosphere from two superthermal electron sources, photoelectrons and plasma sheet electrons, are calculated using a global kinetic model of electron transport in the inner magnetosphere. Peak rates above $10^{10}$ eV cm$^{-2}$ s$^{-1}$ are found for photoelectrons in the midlatitude afternoon region, while the peak deposition rate for plasma sheet electrons only occasionally approaches $10^{9}$ eV cm$^{-2}$ s$^{-1}$, and is typically confined to the morningside. Trapped clouds of plasma sheet electrons, however, are shown to have lasting effects on the structure of topside heat input, as the energetic electrons corotate and slowly transfer their energy to the thermal plasma over a course of days. These energy inputs are compared with other heat sources in the inner magnetosphere. It is concluded that, while other processes can inject large amounts of energy into the ionosphere in spatially and temporally localized regions, photoelectrons are the strongest and steadiest heat source into the topside ionosphere. 

*Keywords:* Topside ionosphere; Superthermal electrons; Heating

## 1. Introduction

Energy deposition to the thermal plasma in the inner magnetosphere is a vital contributor to the global energy balance of the ionosphere–magnetosphere system. For instance, knowledge of the energy precipitation from the magnetosphere into the ionosphere and thermosphere is crucially important for accurate ionospheric prediction. Incorporation of deterministic values of these quantities is a necessary input to any large-scale circulation model. Energy transferred to the thermal plasma in the near-Earth region is conducted down the field lines into the topside ionosphere, where it modifies the thermal, compositional, and optical structures there (Chandler et al., 1988; Kozyra et al., 1990; Comfort et al., 1995). The development of an improved modeling capability for ionospheric specification and prediction requires detailed knowledge of this heat input into the upper atmosphere. In the next millennium, we will see an even greater reliance on satellite communications and radio navigation, necessitating greater accuracy from the current batch

* Corresponding author. Tel.: +1-734-763-6229; fax: +1-734-647-3083.
*E-mail address:* liemohn@engin.umich.edu (M.W. Liemohn).

1364-6826/00/$ - see front matter 
PII: S1364-6826(00)00033-X

of global ionospheric models, and quantifying the magnetospheric heat input is an essential step.

In addition to ionospheric ramifications, inner magnetospheric thermal plasma heating has consequences for upcoming scientific missions, such as IMAGE. Global characterization of the energy deposition to the thermal plasma must be determined before the effects on electron and ion temperatures and global plasma distribution out of the equatorial plane can be addressed. Craven et al. (1991) show considerable structure in the temperatures of the plasmaspheric ions, structure which has not been fully explained but which is almost certainly related to the structure in the energy sources. These issues should be addressed to fully utilize and understand the IMAGE plasmasphere observations.

In this study, one component of the heat input to the inner magnetospheric thermal plasma is considered — the contribution from superthermal electrons. A distinctive feature of the inner magnetosphere is the presence of electrons from a few eV up to a few keV. This population is formed not only due to ionization of the atmospheric neutral atoms and molecules by photoionization, but also due to earthward convection of the warm plasma sheet electrons. Superthermal electrons play a very important role in a large number of ionospheric and plasmaspheric processes, notably thermal plasma heating, and a fairly detailed knowledge of the superthermal electron distribution function is required (see Khazanov et al., 1994 and Khazanov and Liemohn, 1995, for a detailed discussion). Our model of superthermal electron transport calculates the distribution on a global scale throughout the subauroral magnetosphere (Khazanov et al., 1996a, 1998). Here, this model is used to determine the energy flux into the upper ionosphere from the calculated photoelectron and plasma sheet electron distribution functions in the midlatitude region. For perspective, these results are compared to previous calculations of topside heating from other energy sources.

## 2. Model

The column heating rates $P_i$ are found by integrating the Coulomb collision operator between the superthermal electrons and the thermal plasma $S_{e\alpha}$ over velocity space and also along the field line. The linearized version of this integrand has the form

$$S_{e\alpha} = An_e\left\{\frac{m_e}{m_\alpha}\frac{\partial}{\partial E}\left[\frac{\phi}{E} + T_\alpha\frac{\partial}{\partial E}\left(\frac{\phi}{E}\right)\right] + \frac{1}{4E^2}\frac{\partial}{\partial\mu}\left[\left(1-\mu^2\right)\frac{\partial\phi}{\partial\mu}\right]\right\} \quad (1)$$

where $\alpha$ is the thermal plasma species, $\phi = \phi$ ($t$, $E$, $\mu$, $s$, $R_0$, $\varphi$) is the differential flux of superthermal electrons, $t$ is time, $E$ is energy, $\mu$ is the pitch angle cosine, $s$ is distance along the field line, $R_0$ is geocentric distance to the field line in the equatorial plane, and $\varphi$ is magnetic local time around the Earth. The $\mu$ derivative yields nothing to the heating rate integral, and the contribution to each thermal plasma species is roughly equal to the thermal electron heating rate multiplied by the electron-to-ion mass ratio. Therefore, this study will focus on the energy input to the thermal electrons (the largest absorber of superthermal electron energy). From Eq. (1), the localized heating rate $Q$ has the form

$$Q = An_e\left\{\phi(E_{min})\left[1 - \frac{T_e}{E_{min}}\right] + \int_{E_{min}}^{\infty}\frac{\phi}{E}dE\right\} \quad (2)$$

and $P_i$ can be written in terms of this as

$$P_i = \int_{s_0}^{s_i} Q\frac{B_i}{B}ds \quad (3)$$

where the i subscript indicates quantities at the ionospheric boundary and the 0 subscript is for the equatorial plane. The integral only covers half of the flux tube because the energy deposition is shared between the two conjugate footpoints of the field line.

The superthermal electron flux distribution function $\phi$ ($\phi = 2Ef/m^2$) is found by a combination of two time-dependent, kinetic transport models (Khazanov and Liemohn, 1995; Khazanov et al., 1998). Details of this combined model are given in Khazanov et al. (1998), and so only a brief description will be given here. The first model is a field-line calculation that includes all of the atmospheric neutral and ionospheric collisional interactions, ran many times over a grid of latitudes and longitudes. The second model is a bounce-averaged model that includes the effects of cross-field-line drifts. The two models are run simultaneously, sharing information as needed. The field-line model provides the source of the photoelectrons on the dayside, the atmospheric sink of both populations (especially on the nightside), and the secondary electron sources from the precipitating electrons. The energy range extends down to a few electron volts and up to several tens of keV, thus capturing the entire superthermal electron energy range in the calculation. In addition, because the formulation is linear, the two source terms (photoelectrons and plasma sheet electrons) can be solved independently with the results summed after the calculations. This allows us to isolate the heating from each population in order to better examine their influences to topside heating. The magnetospheric thermal plasma is calculated with the model of Rasmussen et al. (1993), also ran simul-

taneously with the superthermal electron models, and the thermospheric and ionospheric inputs are given by the MSIS (Hedin, 1991) and IRI (Bilitza, 1990) models, respectively.

## 3. Results

To begin, two extreme geophysical conditions were imposed in order to quantify the limits of energy deposition from these two superthermal electron populations. Both are steady-state results, meaning the simulations were conducted for several days (48 h of simulation time) and only the final output is reported. The two runs hold the planetary index $K_p$ constant at 1 and at 6, representing low and high geomagnetic activity, respectively. Integrated electron heating rates from Eq. (3) for these two runs are shown in Fig. 1. Note that it is the logarithm of the integrated heating rate that is being presented vs. MLT and magnetic latitude. It is clear that when activity is low, the plasma sheet electrons show only miniscule heating to the ionosphere, and only at higher latitudes. It is also seen that the photoelectrons show a very strong heat input to the topside ionosphere, reaching a maximum in the afternoon sector. Also of interest is the band of heating throughout the nightside at higher latitudes by the photoelectrons during low activity. This is produced by the transport of photoelectrons through the nightside in a restricted band, cut off on the low-latitude side by increased thermal plasma densities and rapid absorption in the evening sector, and cut off at high latitudes by Earthward convection forces from the tail.When activity is increased, however, these patterns

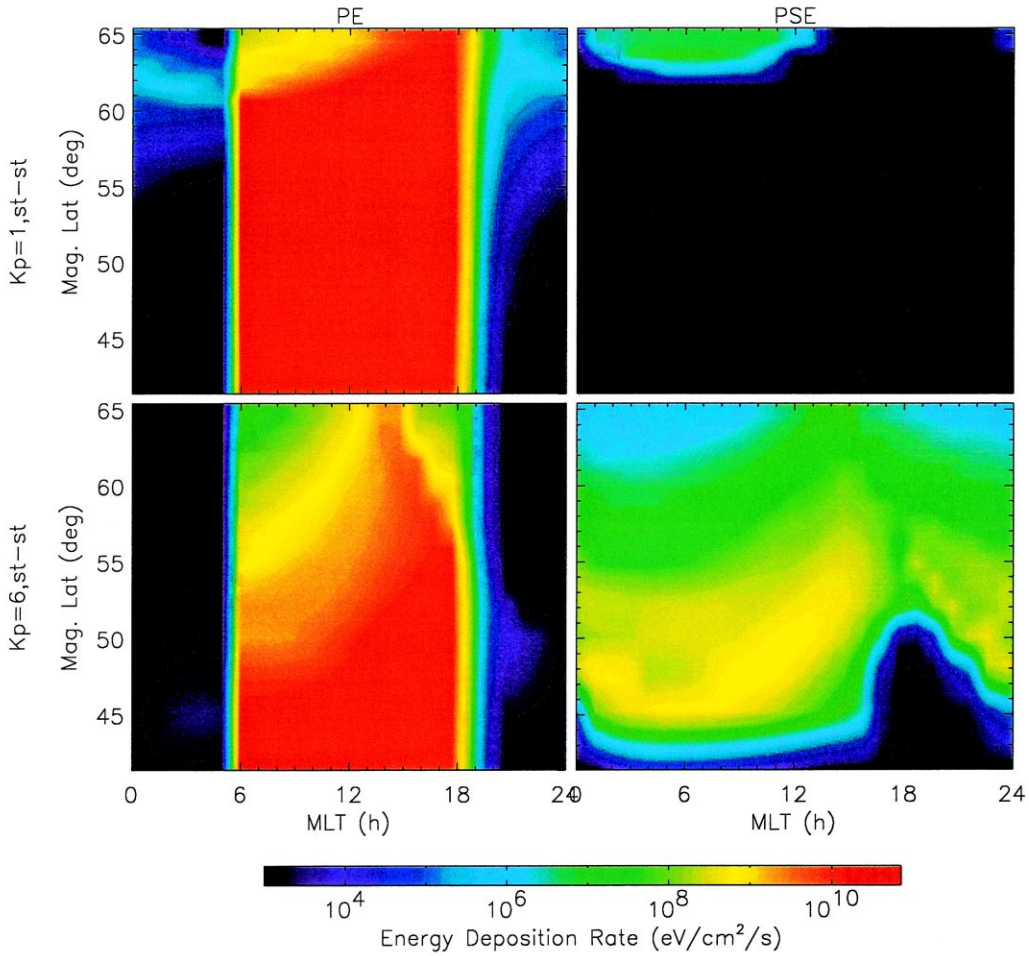


Fig. 1. Contour plot of log $P_i$ (column heating rates in eV $cm^{-2}$ $s^{-1}$) as a function of latitude and MLT for photoelectrons (left panels) and plasma sheet electrons (right panels) for $K_p = 1$ (upper panels) and $K_p = 6$ (lower panels). Note the intensity scale is logarithmic (also in Fig. 4).

change dramatically. The photoelectrons show substantially less heat input into the topside ionosphere, there is no sign of the nightside heating band, and the plasma sheet electrons show heat input at all local times, particularly the morning sector. These energy deposition trends are expected from the change in the convection patterns in the inner magnetosphere. As activity increases, the cross-tail electric field increases and dominates over the corotation field, stripping away the plasmasphere so there is far less thermal plasma to collide with and absorb the energy of the superthermal electrons. Note that the photoelectrons still dominate over much of the dayside, and that there is still an energy deposition minimum in the premidnight region. This dominance is due not only to the difference in flux intensity, but also to the difference in characteristic energy. The photoelectrons have a mean energy of well under 50 eV, while the plasma sheet electrons have a mean energy in the hundreds of eV. Because of the inverse relationship between Coulomb collisions and superthermal electron energy, as seen in Eq. (1), more heat is transferred from the photoelectrons than from the plasma sheet electrons because of their lower particle energies.

Fig. 2 shows line plots of the results in Fig. 1. Note that the photoelectrons and plasma sheet electrons have different MLTs chosen as well as different scales. It is seen that during quiet conditions, the photoelectrons provide a large and steady heat input of a few times $10^{10}$ eV cm$^{-2}$ s$^{-1}$ back down into the dayside ionosphere. Note that this is heating occurring in the magnetosphere and being conducted down, and does not include the local heating from these electrons

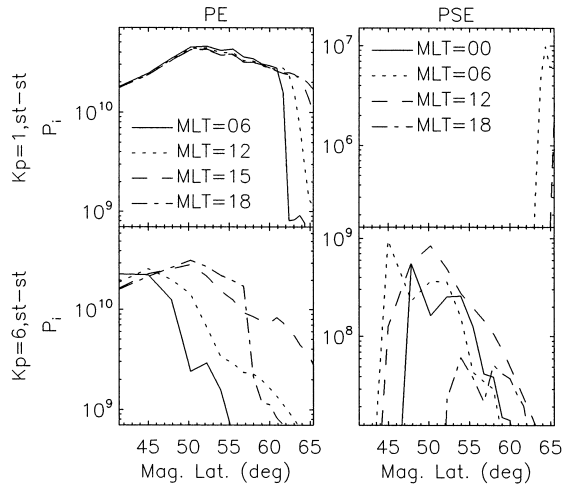


Fig. 2. Column heating rates in eV cm$^{-2}$ s$^{-1}$ versus latitude at several MLTs for photoelectrons (left panels) and plasma sheet electrons (right panels) for $K_p = 1$ (upper panels) and $K_p = 6$ (lower panels).

to the thermosphere and ionosphere near or below the $F_2$ peak. During active times, however, this steady heat source is disrupted by the increased convection. The plasma sheet electron heat input is almost nonexistent during quiet times, but is quite significant during active times.

These limited cases, however, do not show the complex and time-dependent nature of the heating patterns that can arise from a realistic scenario of geomagnetic activity. To examine such a case, the injected cloud-trapping event in January 1991 will be studied. The $K_p$ history during this event is shown in Fig. 3, and during the three peaks in $K_p$, plasma sheet electrons were trapped on closed field lines. Each peak contributed further to the build-up of a cloud of plasma sheet electrons in the inner magnetosphere, a cloud that took days to disperse. This event has been studied both observationally (Burke et al., 1995) and theoretically (Liemohn et al., 1998; Khazanov et al., 1998), and so here we will only discuss the heating to the topside ionosphere from this trapped cloud.

Fig. 4 shows contour plots of log $P_i$ for photoelectrons and plasma sheet electrons during this cloud-trapping event. The first row is immediately following the initial injection event, the second row is during the third (and final) segment of the trapping, the third row is 12 h later, just after the final injection event, and the fourth row is over two days later after the cloud was starting to break up. In reality, the photoelectrons wax and wane on the dayside but do not really lose their strength of energy input to the topside ionosphere. Also, the nightside band of heating is always present for this $K_p$ history. Note that after the initial injection, the heating pattern from the cloud is very localized near midnight. As time progresses, the signature becomes stronger and spread out, but still shows a maximum and a minimum in local time. The corotation of the cloud is seen between the second and third rows as the cloud shifts 12 h of local time, right with the simulation time change. By the final time shown, the degradation of the cloud is evident as the heat

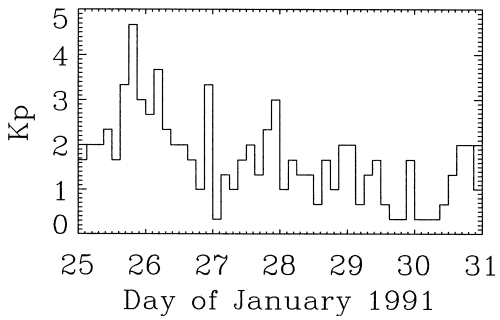


Fig. 3. $K_p$ history during the cloud-trapping event of January 1991.

input away from the peak is greatly reduced and the width of the heated region is narrower. An interesting feature of these plasma sheet electron heating plots is that this $K_p$ history does not allow these particles inside of about $L = 3.5$ (magnetic latitudes of about 55°). The plasma sheet cloud is able to persist much longer than the photoelectrons, which degrade rapidly away from their source region, because of its large characteristic energy compared to the thermal plasma. The energy transfer is far slower than for photo-

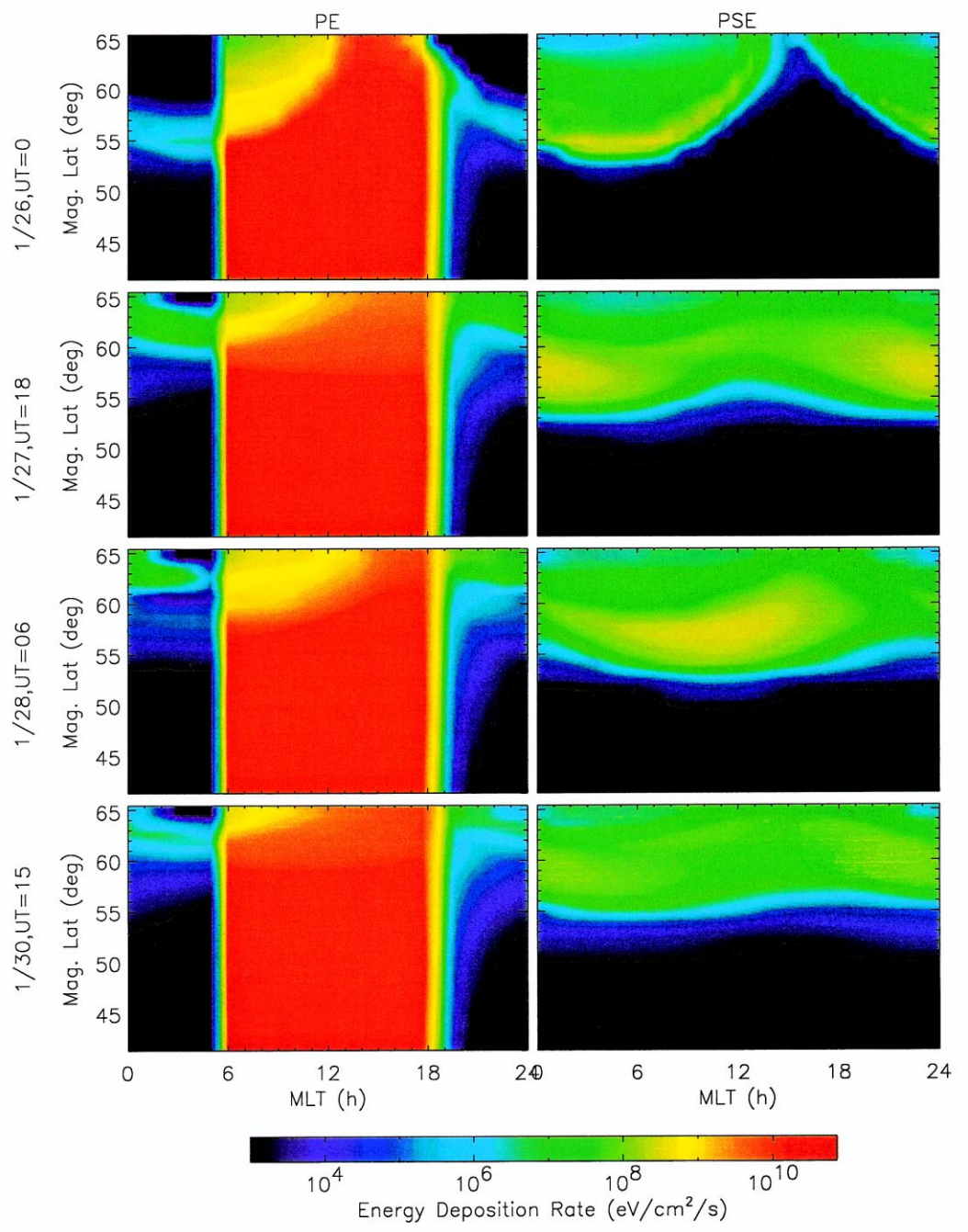


Fig. 4. Contour plot of log $P_i$ (in eV cm$^{-2}$ s$^{-1}$) as a function of latitude and MLT for photoelectrons (left panels) and plasma sheet electrons (right panels) for four times during the cloud-trapping event on January 1991.

electrons, so these trapped plasma sheet electrons simply circle the globe, losing energy at a modest but significant rate to the thermal plasma and thus to the topside ionosphere.

Fig. 5 shows line plots at constant MLT of the contours in Fig. 4. The photoelectron results clearly show a persistent dawn-to-dusk asymmetry in the high-latitude dayside heating rate to the topside ionosphere. The plasma sheet electrons begin with a large peak in heating from the initial injection, which becomes a round-edged cloud by the third injection, and slowly degrades from there.

## 4. Discussion

Energy fluxes into the topside ionosphere have been presented from two superthermal electron sources: photoelectrons and plasma sheet electrons. Peak rates of a few times $10^{10}$ eV cm$^{-2}$ s$^{-1}$ were found for photoelectrons, mostly on the dayside, and max rates of close to $10^{9}$ eV cm$^{-2}$ s$^{-1}$ were found for plasma sheet electrons, mostly at higher latitudes on the morningside. To put them into perspective, Table 1 lists expected peak integrated heating rates from various magnetospheric energy sources, and Fig. 6) shows schematics of the regions where these peak values typically occur. The first two entries are photoelectrons and plasma sheet electrons, with values from this study. Note that the photoelectron heat inputs match previously calculated values (Khazanov and Gefan, 1982; Liemohn and Khazanov, 1995). Fig. 6(a) and (b) illustrate where these maximum heat rates are usually deposited into the topside ionosphere.

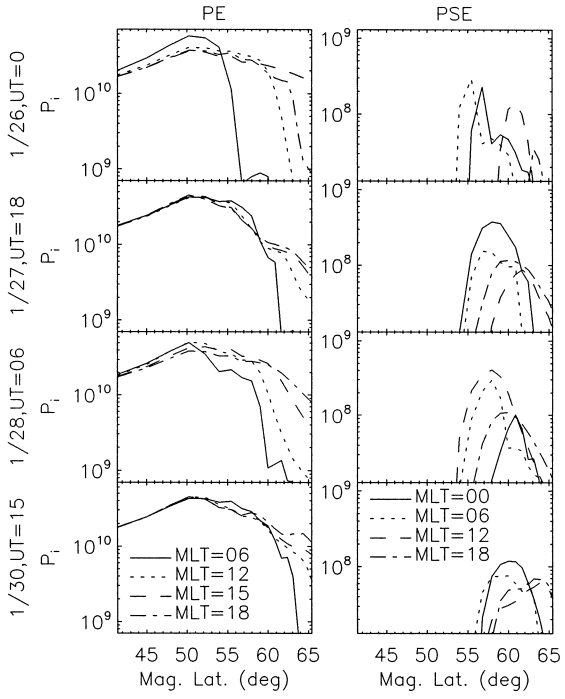


Fig. 5. Column heating rates in eV cm$^{-2}$ s$^{-1}$ versus latitude at several MLTs for photoelectrons (left panels) and plasma sheet electrons (right panels) for four times during the cloud-trapping event on January 1991.

Like electrons, plasma sheet and ring current ions can also deposit energy to the thermal plasma. Even with the mass ratio acting to prevent efficient energy transfer, the speeds of ring current ions and thermal electrons are close enough to allow transfer to occur, and thus deposition to the topside ionosphere is expected from these populations (Kozyra et al., 1987, 1990; Jordanova et al., 1997). It is interesting to note that photoelectrons are still the dominant process on the dayside with the inclusion of hot ion deposition, and that the plasma sheet electrons and ions are actually complementary in their regions of energy deposition. In Fig. 6(c), the gap in the prenoon sector does not indicate that no heating due to ring current ions occurs here, it is just that there is a minimum at this location in the heating from energetic ions.

In addition to particle effects, plasma waves can also be a source of energy to the topside ionosphere. In particular, ion cyclotron waves excited in the ring current region get damped when they propagate in the plasmasphere, and the energy carried by the waves is often transferred to the background thermal plasma (Khazanov and Chernov, 1988; Konikov et al., 1989). These studies used the quasi-linear approximation to calculate the collision terms for the hydrodynamic equations, showing that the attenuation of these waves substantially heats the cold electrons in the outer plasmasphere. When thermal electrons are in resonance with ion cyclotron waves, the field-aligned component of the wave electric field accelerates the thermal electrons in the parallel direction. This selective heating of one degree of freedom results in a temperature aniso-

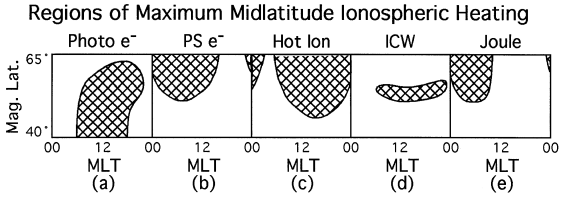


Fig. 6. Schematic of the regions where the maximum energy deposition might occur (see Table 1) for (a) photoelectrons, (b) plasma sheet electrons, (c) plasma sheet/ring current ions, (d) ion cyclotron waves, and (e) convection-driven Joule heating. The vertical axis ranges over the midlatitudes and the horizontal axis ranges from $MLT = 0$ to 24 h (as in Figs. 1 and 4.

Table 1
Maximum energy deposition rates from various sources

| Energy source | Maximum rate (eV $cm^{-2}$ $s^{-1)}$ | Literature references |
|---|---|---|
| Photoelectrons | $10^9$–$10^{11}$ | This study; Khazanov and Gefan (1982) and Liemohn and Khazanov (1995) |
| Plasma sheet electrons | $10^7$–$10^9$ | This study |
| Ring current/plasma sheet ions | $10^8$–$10^{10}$ | Kozyra et al. (1987) and Jordanova et al. (1997) |
| Ion cyclotron waves | $10^9$–$10^{11}$ | Khazanov and Chernov (1988) and Konikov et al. (1989) |
| Joule heating | $10^9$–$10^{10}$ | Krymskiy (1990) |

tropy in the thermal electrons. An identical situation takes place for the cold ions, as a result of induced scattering processes. These temperature anisotropies could be then reduced by particle-particle collisions, leading to warm Maxwellian distributions (Konikov, 1990; Gamayunov et al., 1991). Another energy channel is wave-wave interactions, where additional modes are excited that more readily deposit their energy to the thermal plasma. One such coupling mechanism is the generation of lower hybrid waves (LHWs). LHW excitation is a widely discussed mechanism of interaction between plasma species in space. Possible mechanisms of lower hybrid wave excitation include accelerated electron beams (Maggs, 1976; Chang and Coppi, 1981), anomalous Doppler resonance of waves with precipitating electrons (Omelchenko et al., 1994), the lower hybrid drift instability in inhomogeneous plasmas (Davidson et al., 1977; Huba et al., 1978), and also by the relative drifts caused by the ion cyclotron waves (Khazanov et al., 1996b, 1997). Such waves are particularly interesting because they couple well to both electrons and ions, providing an additional energy channel to the thermal plasma. However the energy is transferred to the thermal plasma, this heat input can be substantial. It is quite localized, though, restricted to the region of interaction between the ring current and the plasmasphere, and is often patchy within this band (Jordanova et al., 1997). Fig. 6(d) shows the typical location of maximum wave growth for ion cyclotron waves.

The final form of heating to be considered is Joule heating following magnetospheric convection intensification. According to Krymskiy (1990), thermal ions can be heated during disturbances as a result of the process of gyrorelaxation heating (Braginskiy, 1965), which consists of the following: as the azimuthal current intensifies, the plasma is compressed; the magnetic field increases as $B \propto n$; and the thermal ion transverse energy increases. Redistribution of energy over three degrees of freedom due to the collisions is an irreversible process, and it is related to the dissipation and liberation of heat. Thus the viscous and Joule dissipation during periods of convection intensification provide for the heating of the plasma, which facilitates the creation of a warm zone on the periphery of the plasmasphere (Gringauz and Bezrukikh, 1976). This level rivals that of the photoelectrons, but is not generally coincident with it (see Fig. 6). This heating typically occurs on the nightside, particularly in the post-midnight region, and only during the growth phase of storms and substorms.

This analysis indicates that superthermal electrons play a significant role in providing energy input to the topside ionosphere. In the context of other heat sources, the photoelectrons are especially vital to providing energy into the dayside upper ionosphere, and the plasma sheet electrons to the morningside after injection events. However, as indicated in Figs. 4 and 5, the plasma sheet electrons can become trapped and last for several days in the inner magnetosphere, long after the injection disturbance has subsided. This is not the case for some other energy sources, however, such as Joule heating, which also provides heat input to the morning sector but will only be an influencing factor during the buildup of disturbed conditions.

## Acknowledgements

This work was supported by National Science Foundation (NSF) grants ATM-9711381, ATM-9710326, and ATM-9800830, and National Aeronautics and Space Administration (NASA) grants NAG-4771, NAG5-6976, and NCC8-181.

## References

Bilitza, D., 1990. Progress report on IRI status. Advances in Space Research 10 (11), 3–15.

Braginskiy, S.I., 1965. Leontovich, M.A. (Ed.), Reviews of Plasma Physics, vol. 1. Consultants Bureau, pp. 3–115 (Chapter 1).

Burke, W.J., Rubin, A.G., Hardy, D.A., Holeman, E.G., 1995. Banded electron structures in the plasmasphere. J. Geophys. Res. 100, 7759–7769.

Chandler, M.O., Kozyra, J.U., Horwitz, J.L., Comfort, R.H.,

Brace, L.H., 1999. Modeling of the thermal plasma in the outer plasmasphere — a magnetospheric heat source. In: Moore, T.E., Waite Jr, J.H. (Eds.), Modeling Magnetospheric Plasma, Geophysical Monograph Series, vol. 44. American Geophysical Union, pp. 101–105.

Chang, T., Copi, B., 1981. Lower hybrid acceleration and ion evolution in the subauroral region. Geophysical Research Letters 8, 1253–1256.

Comfort, R.H., Richards, P.G., Craven, P.D., Chandler, M.O., 1995. Problems in simulating ion temperatures in low density flux tubes. In: Horwitz, J.L., Singh, N., Burch, J.L. (Eds.), Cross-Scale Coupling in Space Plasmas, Geophysical Monograph Series, vol. 93. American Geophysical Union, pp. 155–160.

Craven, P.D., Comfort, R.H., Gallagher, D.L., West, R., 1991. A study of the statistical behavior of ion temperatures from DE 1/RIMS. In: Wilson, G.R. (Ed.), Modeling Magnetospheric Plasma Processes, Geophysical Monograph Series, vol. 62. American Geophysical Union, pp. 173–182.

Davidson, R.C., Gladd, N.T., Wu, C.S., Huba, J.D., 1977. Effects of finite plasma beta on the lower-hybrid-drift instability. Physics of Fluids 20, 301–312.

Gamayunov, K.V., Krivorutsky, E.N., Khazanov, G.V., 1991. Hydrodynamic description of magnetosphere plasma with due regard to the wave activity of Alfvén and fast magnetosonic waves. Planetary and Space Science 39, 1097–1105.

Gringauz, K.I., Bezrukikh, V.V., 1976. Earth's plasmasphere. Geomagnetism and Aeronomy 17, 784–800.

Hedin, A.E., 1991. Extension of the MSIS thermospheric model into the middle and lower atmosphere. Journal of Geophysical Research 96, 1159–1173.

Huba, J.D., Gladd, N.T., Papadopoulos, K., 1978. Lower hybrid drift turbulence in the distant magnetotail. Journal of Geophysical Research 83, 5217–5226.

Jordanova, V.K., Kozyra, J.U., Nagy, A.F., Khazanov, G.V., 1997. Kinetic model of the ring current–atmosphere interactions. Journal of Geophysical Research 102, 14,279–14,291.

Khazanov, G.V., Chernov, A.A., 1988. The effect of Alfvén and fast magnetosonic turbulence on the heating of electrons and kinetic coefficients of the plasmasphere. Ionospheric Investigations (in Russian) 44, 100–107.

Khazanov, G.V., Gefan, G.D., 1982. The kinetics of ionosphere–plasmasphere transport of superthermal electrons. Solar–Terrestrial Physics 19, 65–80.

Khazanov, G.V., Krivorutsky, E.N., Moore, T.E., Horwitz, J.L., Liemohn, M.W., 1997. Lower hybrid oscillations in multicomponent space plasmas subjected to ion cyclotron waves. Journal of Geophysical Research 102, 175–184.

Khazanov, G.V., Liemohn, M.W., 1995. Non-steady-state ionosphere–plasmasphere coupling of superthermal electrons. Journal of Geophysical Research 100, 9669–9681.

Khazanov, G.V., Liemohn, M.W., Kozyra, J.U., Moore, T.E., 1998. Inner magnetospheric superthermal electron transport: photoelectron and plasma sheet electron sources. Journal of Geophysical Research 103, 23,485–23,501.

Khazanov, G.V., Moore, T.E., Liemohn, M.W., Jordanova, V.K., Fok, M-C., 1996a. Global, collisional model of high-energy photoelectrons. Geophysical Research Letters 23, 331–334.

Khazanov, G.V., Moore, T.E., Krivorutsky, E.N., Horwitz, J.L., Liemohn, M.W., 1996b. Lower hybrid turbulence and ponderomotive force effects in space plasmas subjected for large-amplitude low-frequency waves. Geophysical Research Letters 23, 797–800.

Khazanov, G.V., Neubert, T., Gefan, G.D., 1994. Kinetic theory of ionosphere–plasmasphere transport of suprathermal electrons. IEEE Transactions in Plasma Science 22, 187–198.

Konikov, Yu.V., 1990. Hydrodynamic equations in 16-moment approximation allowing for interactions of thermal electrons with ion cyclotron waves in the Earth's outer plasmasphere. Planetary and Space Science 38, 709–719.

Konikov, Yu.V., Gorbachev, O.A., Khazanov, G.V., Chernov, A.A., 1989. Hydrodynamical equations for thermal electrons taking into account their scattering on ion cyclotron waves in the outer plasmasphere of the Earth. Planetary and Space Science 37, 1157–1168.

Kozyra, J.U., Shelley, E.G., Comfort, R.H., Brace, L.H., Cravens, T.E., Nagy, A.F., 1987. The role of ring current $O^+$ in the formation of stable auroral red arcs. Journal of Geophysical Research 92, 7487–7502.

Kozyra, J.U., Valladares, C.E., Carlson, H.C., Buonsanto, M.J., Slater, D.W., 1990. A theoretical study of seasonal and solar cycle variations of stable aurora red arcs. Journal of Geophysical Research 95, 12219–12234.

Krymskiy, P.F., 1990. Azimuthal currents and heating of the plasma near plasmapause during periods of disturbances. Geomagnetism and Aeronomy 30, 633–639.

Liemohn, M.W., Khazanov, G.V., 1995. Non-steady-state coupling processes in superthermal electron transport. In: Horwitz, J.L., Singh, N., Burch, J.L. (Eds.), Cross-Scale Coupling in Space Plasmas, Geophysical Monograph Series, vol. 93. American Geophysical Union, pp. 181–191.

Liemohn, M.W., Khazanov, G.V., Kozyra, J.U., 1998. Banded electron structure formation in the inner magnetosphere. Geophysical Research Letters 25, 877–880.

Maggs, J.E., 1976. Coherent generation of VLF hiss. Journal of Geophysical Research 81, 1707–1724.

Omelchenko, Yu.A., Shapiro, V.D., Shevchenko, V.I., Ashour-Abdalla, M., Schriver, D., 1994. Modified lower hybrid fan instability excited by precipitating auroral electrons. Journal of Geophysical Research 99, 5965–5975.

Rassmussen, C.E., Guiter, S.M., Thomas, S.G., 1993. Two-dimensional model of the plasmasphere: refilling time constants. Planetary and Space Science 41, 35–42.